

## Locomotion modeling of a triangular closed-chain soft rolling robot<sup>☆,☆☆</sup>

Jiangbei Wang, Yanqiong Fei\*, Zhaoyu Liu

*Research Institute of Robotics, Shanghai Jiao Tong University, Shanghai 200240, China*



### ARTICLE INFO

**Keywords:**

Soft robotics  
Rolling locomotion  
Pneumatic artificial muscles  
Dynamics  
State-space model

### ABSTRACT

This paper presents a novel triangular closed-chain soft rolling robot. The proposed robot uses the least number of soft actuators (i.e. three) among current closed-chain soft rolling robots and can achieve faster rolling locomotion. To verify its feasibility in theory, we build a state-space model for simulating its rolling locomotion based on the continuum deformation and the rolling dynamics. Different from previous pseudo-rigid and finite element models, this model is fully analytical and continuous. To validate this model, we conduct experiments of rolling locomotion with a prototype constructed by three Curl Pneumatic Artificial Muscles (CPAMs). The results show that the proposed robot can roll forward with an average velocity of 20–21 mm/s on level ground and 12–13 mm/s on 8° inclined ground. The error of the mass center trajectories and average velocities between the simulation and experiment is within 10%. The proposed soft robot can be expanded into parallel or tetrahedron morphology to enable the steering movement, and it has potential applications in the space exploration and medical operation.

### 1. Introduction

In recent years, soft robotics have been increasingly attracting interest of researchers and engineers. Soft robots are created by applying soft materials such as the elastomers [1], fabrics [2], shape memory alloy [3] and electroactive polymers [4] to robots and actuating them to perform motion of continuous infinite degree of freedom (DOF). Compared with conventional rigid robots, soft robots are more flexible, adaptable and safe, which allows them to interact with unstructured environments better and perform tasks in more dynamic manners [5]. According to their functions, soft robots can be classified into four categories: locomotion, manipulation, assistance and sensing. Most locomotion soft robot is inspired by the nature creatures such as the octopus [6], starfish [7], fish [8], snake [9], spider [10], inchworm [11] and caterpillar [12]. Their locomotion generally includes swimming, crawling, jumping and rolling. This work mainly researches on the rolling locomotion.

To achieve locomotion, most of the soft rolling robots are designed into a closed-chain structure like a wheel except some special cases such as the caterpillar-inspired GoQBot [12]. The rolling locomotion is based on a succession of stable and unstable states. By deformation, the closed chain can vary its profile and mass center. When the gravity force at the mass center is out of the supporting points, i.e. in an unstable state, the robot will perform rolling movements until it goes into a new stable state. After that, the robot can continue to deform for constantly rolling.

Such rolling motion requires non-symmetric deformation of the closed chain. Therefore, at least three soft actuators are needed for con-

structing the soft rolling robot. In previous studies, such robots usually use four [13,14], six [9], eight [15–17] or more [18–20] soft actuators to achieve the rolling locomotion. Although more actuators can ensure more smooth movements, they also make the robot bulky and heavily tethered by the pneumatic pipes or power wires. In addition, more actuators consume longer actuation time per locomotion cycle and thus reduce the average moving speed.

In modeling the rolling locomotion, some previous studies developed pseudo-rigid-body model [16], particle-based model [20,21], finite element model [17] and finite-mode model [13]. The first three models discretize the continuous soft robot into finite elements and thus their accuracy is highly dependent on the number of elements. For large deformation, many elements are needed, which consume more calculating time. The finite-mode model is a continuous method, which assumes the robot's deformation conforms with a series of certain shapes. This model is very useful in engineering due to its simplicity and effectiveness. However, this method requires reasonable deformation assumptions, which would be difficult for some unknown cases. Therefore, it is necessary to build an analytical model based on as fewer assumptions as possible.

To address these problems, we develop a new lightweight soft rolling robot by using only three Curl Pneumatic Artificial Muscles (CPAMs). Its locomotion dynamics are modeled, and the real locomotion performances are also tested by experiments. The proposed robot has smaller size and lower weight than some previous closed-chain soft rolling robots [13,17,19,20] and can achieve faster rolling locomotion (with speed of 20–21 mm/s or 10% of the robot's size per second on

\* This paper was recommended for publication by Associate Editor Mokrane Boudaoud.

\*\* This work was supported by the National Natural Science Foundation of China under Grant nos. 51475300 and 51875335, Joint fund of the Ministry of Education under Grant no. 18GFA-ZZ07-171.

\* Corresponding author.

E-mail address: [fyq@sjtu.edu.cn](mailto:fyq@sjtu.edu.cn) (Y. Fei).

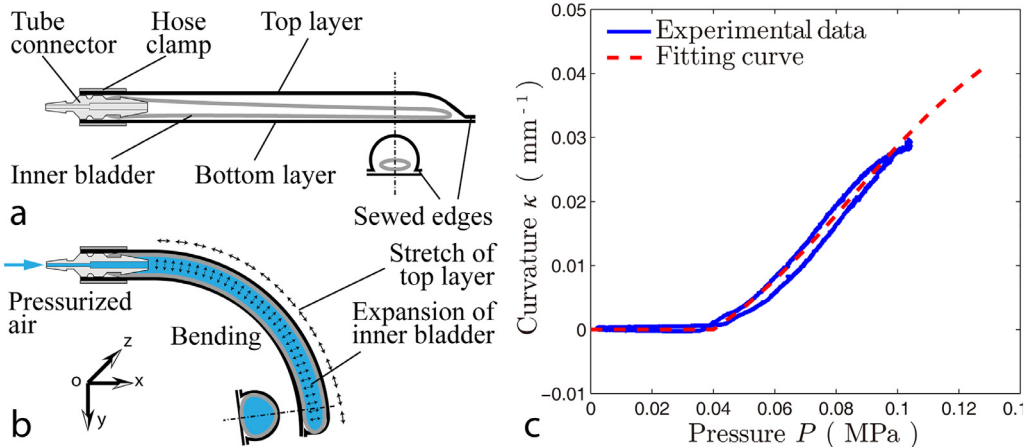


**Fig. 1.** Structure and characteristic of the Curl Pneumatic Artificial Muscle (CPAM). (a) Initial state. (b) Bending state. (c) Free bending curvature with respect to inflating pressure.

level ground) than the typical soft rolling robots that exhibit speed of 5.23 mm/s (6.5% of size per second) [9], 6.8 mm/s (6.8% of size per second) [15], and 4 mm/s (2% of size per second) [22]. The model can predict motion of the robot effectively. It is a state-space model based on the continuous deformation and the rolling dynamics, which is very different from some previous discrete models such as the pseudo-rigid-body model [16], particle-based model [20,21], finite element model [17]. In addition, this model is free of the deformation mode assumptions [13].

## 2. Robot design

In this section, structure design of the proposed soft robot is presented. The used CPAM soft actuator and its characterization are introduced first. Then, structure and dimensions of the robot are illustrated.

### 2.1. The soft actuators

The proposed soft robot is actuated by three Curl Pneumatic Artificial Muscles (CPAMs), which perform bending by filling fabric-encircled bladder with pressurized air. This type of soft actuators have been commonly applied in soft robots and exoskeletons [23–25]. As shown in Fig. 1a, the CPAM is designed as sandwich structure, i.e. the inner latex bladder is sandwiched between the top and bottom fabric layers. The bottom layer made from cotton & linen fabric is plain and unstretchable while the top layer made from polyester & latex fabric is transversely ( $z$ -axially) arched and longitudinally ( $x$ -axially) elastic. When the CPAM is pressurized, expansion of the bladder is radially (in  $yoz$  plane) constrained by the top layer, longitudinally constrained by the bottom layer and only allowed to bend by stretch of the top layer, as shown in Fig. 1b. To form a closed air chamber, the top and bottom layers are sewed together at the two side edges and the distal end and plugged by a tube connector at the proximal end, as shown in Fig. 1a. Each CPAM can actuate one edge of the soft robot to bend unidirectionally.

To characterize the CPAM's bending behavior, the free bending test is conducted, which is to obtain the relationship between the inflating pressure and the bending curvature when the bending moment is zero. The pressure and curvature are measured by a pressure sensor (XGZP6847200KPG, 0–200 kPa, 0–5 V) and a flex sensor (FS-L-0095-103-ST, Spectrasymbol Inc.) respectively. The experimental data are fitted with a horizontal segment  $\kappa = 0$  and a cubic curve  $P = f(\kappa)$ , as shown in Fig. 1c. It can be seen that when the pressure is less than 0.041 MPa, the curvature is zero, which is caused by initial expansion of the inner bladder. The best fitting cubic curve is expressed by Eq. (1), which will

**Table 1**

Parameters of the proposed triangular closed-chain soft robot.

Parameters	Description	Value
$L$	Length of the edges	200 mm
$W$	Width of the soft robot	210 mm
$l_a$	Length of the soft actuators	170 mm
$w_a$	Width of the soft actuators	25 mm
$d$	Distance between soft actuators	30 mm
$t_a$	Thickness of the soft actuators	17 mm
$t_p$	Thickness of the PVC membrane	0.3 mm
$m$	Total mass of the soft robot	110 g

be used in locomotion modeling of the proposed soft robot.

$$f(\kappa) = 0.041 + 3.374\kappa - 70.241\kappa^2 + 1359.551\kappa^3 \quad (1)$$

where units of  $\kappa$  and  $f(\kappa)$  are mm<sup>-1</sup> and MPa respectively.

### 2.2. The soft rolling robot

The proposed novel soft rolling robot is constructed by mounting three CPAM soft actuators on one side of a transparent PVC membrane (Fig. 2a) and then folding the membrane into a triangular prism with the CPAM-mounted surface as the inner surface (Fig. 2b). Axes of the three CPAMs stagger with each other to prevent the assemble interference between them. In plane, the soft robot is seen as a triangular closed-chain with the CPAMs mounted on the inner side of each edge (Fig. 2c). Upon pressurization, the CPAMs can actuate the edges to bend independently. Thickness of the membrane is so small (about 0.3 mm) that its bending resistance to the CPAMs can be neglected. Therefore, in the locomotion modeling, the edge bending is analyzed as the CPAM bending.

Parameters of the proposed robot shown in Fig. 2 are listed in Table 1. The edge length is designed a little longer than the actuator's length in order to leave space for the air pipe. Width of the robot is designed large enough to prevent lateral rollover during rolling locomotion. Distance between the soft actuators is a little larger than their width for avoiding the interference between them, as shown in Fig. 2b. Thinner soft actuators are preferred to reduce their influence on the edges' contact. Due to only three lightweight CPAMs used, total mass of the proposed robot (110 g) is less than that of some previous soft rolling robots [13,17,19,20] that use more than three of other soft actuators.

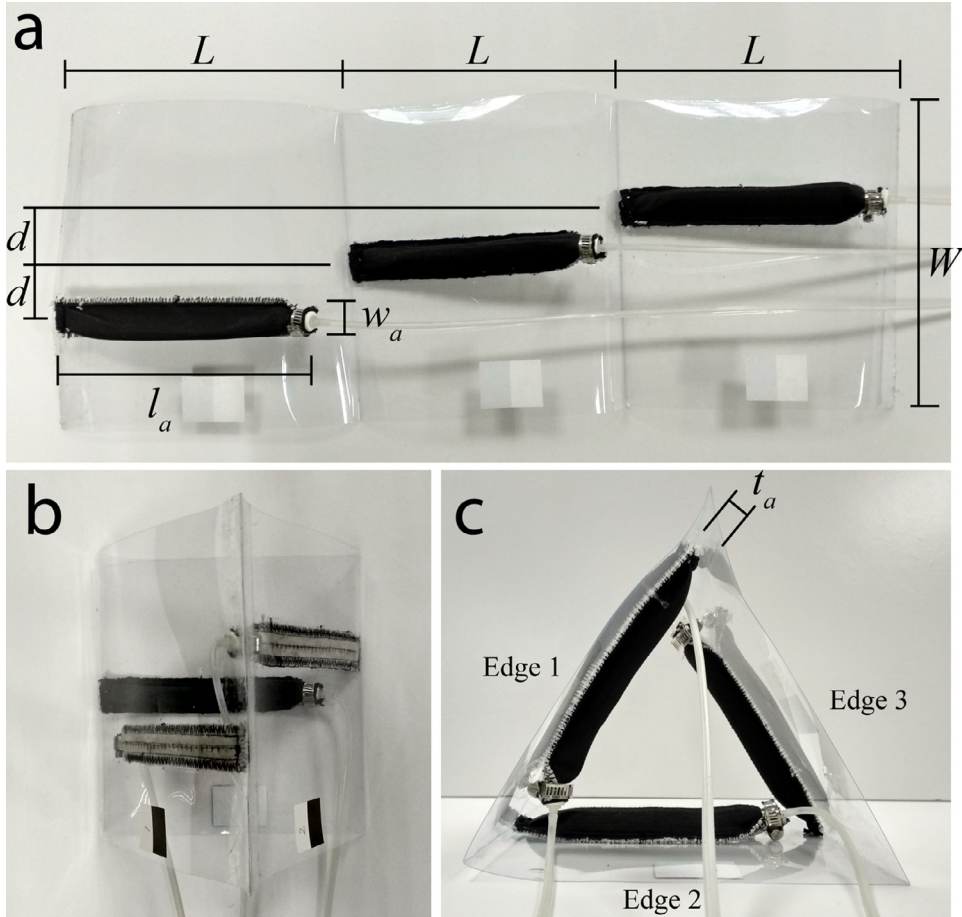


**Fig. 2.** Construction and dimension of the triangular closed-chain soft robot. (a) unfolded top view. (b) folded top view. (c) side view.

### 3. Locomotion modeling

#### 3.1. Overview

Most of current soft rolling robots perform locomotion based on variation of the profile and mass center [9,13–20,22], and so does the proposed robot. Fig. 3a shows that the proposed triangular closed-chain soft robot deforms by inward bending of the three edges to achieve rolling locomotion. First, Edge 1 is actuated to bend slightly to stiffen itself (②). Then, Edge 2 is actuated to bend greatly to gather its two ends that support the whole robot (③). Because Edge 1 is stiffened and Edge 3 not, bending of Edge 2 will lead to asymmetric deformation of the whole robot. When Edge 2's two ends are gathered close enough, the robot's mass center will go out of the two supporting points, and thus the robot will roll forward (③–④). After rolling, Edge 3 becomes the bottom edge in replace of Edge 2 (⑤), and then the robot restores to its undeformed state (⑤–⑥). Therefore, the rolling locomotion is decomposed into four phases: stiffening (①–②), gathering (②–③), rolling (③–④) and releasing (④–⑥). It should be noted that during the releasing phase, Edge 2 is released in advance of Edge 1 in order to expand the supporting area of Edge 3 instantly and thus prevent back rolling.

The proposed robot can roll by  $120^\circ$  and move forward by length of an edge per locomotion cycle (①–⑥) in the ideal conditions that 1) during the gathering phase, the front supporting point is anchored and the rear one shifts forward, 2) during the rolling phase, the robot rolls along Edge 3 without sliding. The first assumption is reasonable because the asymmetric deformation makes the robot's mass center closer to the front supporting point, and thus the front point produces larger normal and frictional forces than the rear. The second assumption can also be

achieved if the frictional coefficient between the edges and ground is large enough.

From the analysis above, the proposed soft rolling robot has several advantages over previous ones: 1) only three soft bending actuators are needed, which is less than previous studies [9,13–20,22] and thus can simplify the actuation, 2) these soft actuators bend inward (i.e. deform concavely) instead of outward (i.e. deform convexly) [9,17], which allows them to be installed inside of the edges and reduces size of the robot, 3) in unactuated state, the triangular soft robot can settle on ground (especially on slope) stably due to its plain side surfaces, which is different from the wheel-like ones.

In addition, the proposed triangular soft robot can also be expanded into a parallel mechanism to enable the steering motion (Fig. 3b) or a tetrahedron mechanism to achieve the multi-direction movement (Fig. 3c). In the former, the two parallel groups of actuators are pressurized differentially to produce a turning angle after a rolling locomotion cycle. In the latter, the robot is seen as four planar triangular ones and can move in triple-directions. The soft actuators used in these 3D mechanisms are both six, still less than some planar soft rolling robots [15–20,22]. The steering and multi-direction movements can enhance maneuverability of the robot and thus make it more practical in applications of space exploration. Due to its flexibility, the robot is adaptable to unstructured environments such as ruins. By applying some intelligent materials such as the Electro-Active Polymers (EAP) [26], the robot can be designed smaller and may have potential applications in surgery such as the capsule endoscope [27]. This research mainly focuses on the modeling, simulation and experiment of the planar triangular closed-chain robot, aimed to verify its feasibility of rolling locomotion in theory and experiment, and make a foundation for further development of the parallel and tetrahedron ones.

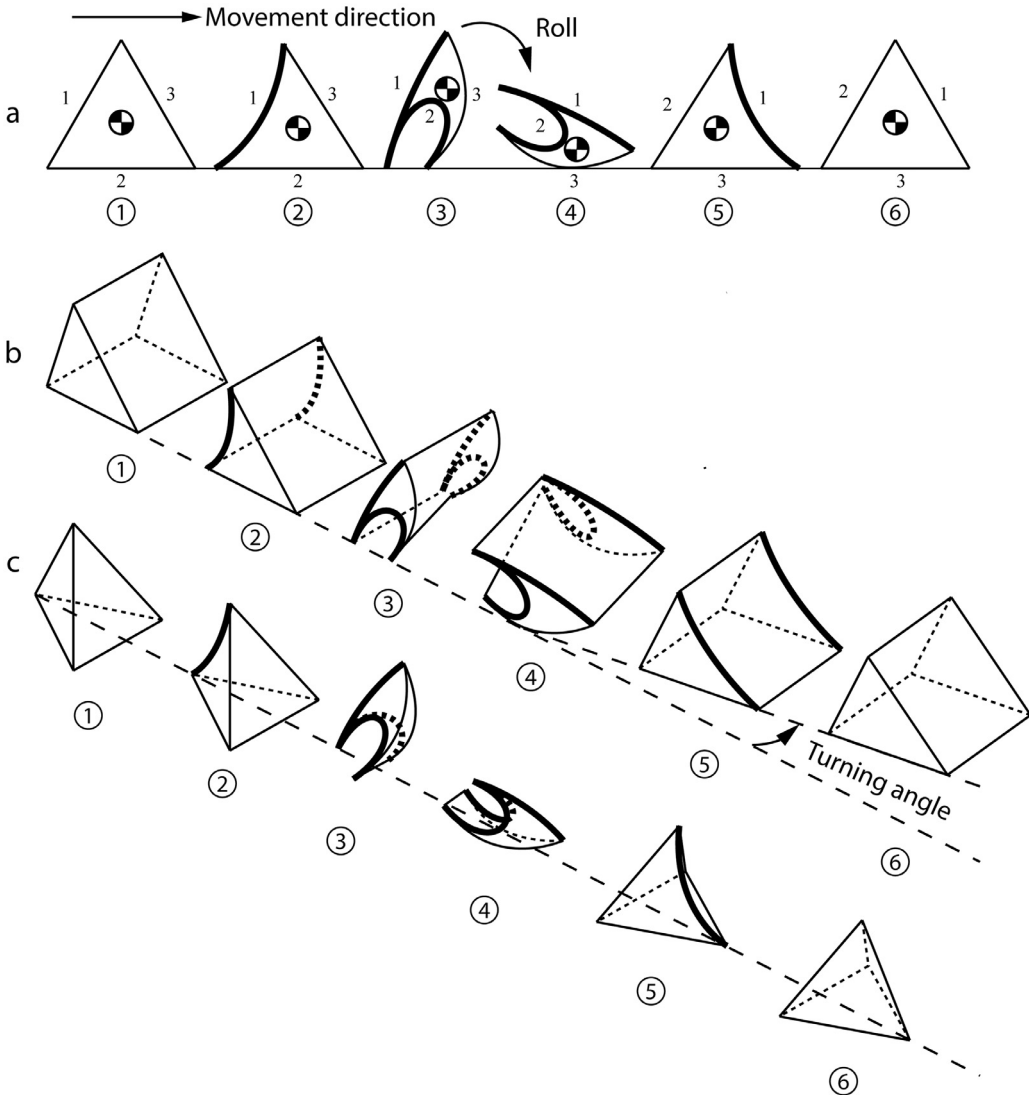


**Fig. 3.** Rolling locomotion cycle of the triangular closed-chain soft robot, in which the thinner and thicker curves indicate the unactuated and bending-actuated edges respectively. (a) Straight motion based on planar mechanism (b) Steering motion based on parallel mechanism (c) Tetrahedron mechanism for multi-direction movements. ① initial state ② Edge 1 bends to stiffen itself ③ Edge 2 bends to gather its two ends ④ the robot rolls due to gravity ⑤-⑥ the robot restores to undeformed state.

Rolling locomotion of the proposed soft robot is modeled in two stages: 1) the deformation, in which the robot's profile, mass center and gyration radius vary with the actuation input such as the inflating pressure of each soft actuator; 2) the rolling, in which the robot contacts with and rolls on the ground due to the deformation. Combining the two stages, a simulation scheme for the robot's rolling locomotion is built based on the state-space model.

### 3.2. Deformation analysis

The proposed soft robot achieves deformation by bending actuation of the three edges. Here, three Curl Pneumatic Artificial Muscles (CPAMs) are used as the soft bending actuators. The aforementioned Eq. (1) obtained by the free bending experiment describes the portion of the inflating pressure consumed by the deformation (i.e. the bending curvature  $\kappa$ ) of the CPAM. The other portion of the inflating pressure contributes to producing the bending moment that is calculated by multiplying the pressure by the cross-section static moment of the CPAM according to the theory of mechanics. Combining the bending deformation with the bending moment of the CPAM yields Eq. (2). It describes the

bending behavior of each actuator (numbered as  $i = 1, 2, 3$ ), indicating the relationship between the local bending moment  $M_i$ , the local bending curvature  $\kappa_i$  and the inflating pressure  $P_i$ . For each actuator with a certain length  $L$ , the bending moment and curvature vary along the arc length coordinate  $s$  ( $0 \leq s \leq L$ ), denoted as  $M_i(s)$  and  $\kappa_i(s)$  respectively. To describe the outline of the soft actuator, a Cartesian coordinate system  $x_{ti}-o_i-y_{ti}$  is set with its origin  $o_i$  located at the actuator's end and the  $x_{ti}$  axis aligned with the tangent direction (Fig. 4a), which is called the actuator's reference frame. In this frame, any point's coordinate  $t^i r_i(s)$  along the actuator and its deflection angle  $\theta_i(s)$  can be obtained according to Eqs. (4) and (3) respectively.

$$M_i = S_p [P_i - f(\kappa_i)] \quad (2)$$

$$\theta_i(s) = \int_0^s \kappa_i(s) ds \quad (3)$$

$$t^i r_i(s) = \int_0^s [\cos \theta_i(s), \sin \theta_i(s)]^T ds \quad (4)$$

where  $i = 1, 2, 3$  is each actuator's number.  $S_p$  is the cross-section static moment of the soft actuator with respect to the unstretchable bottom

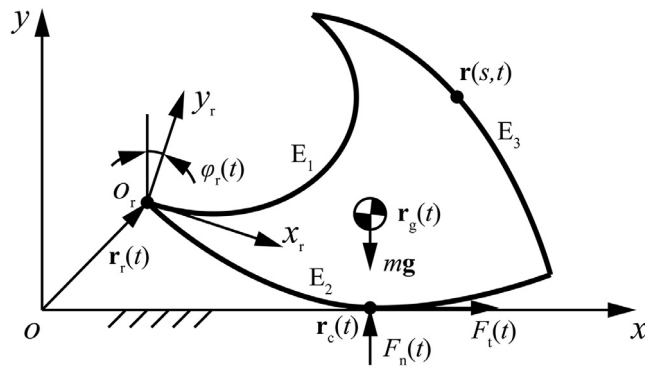
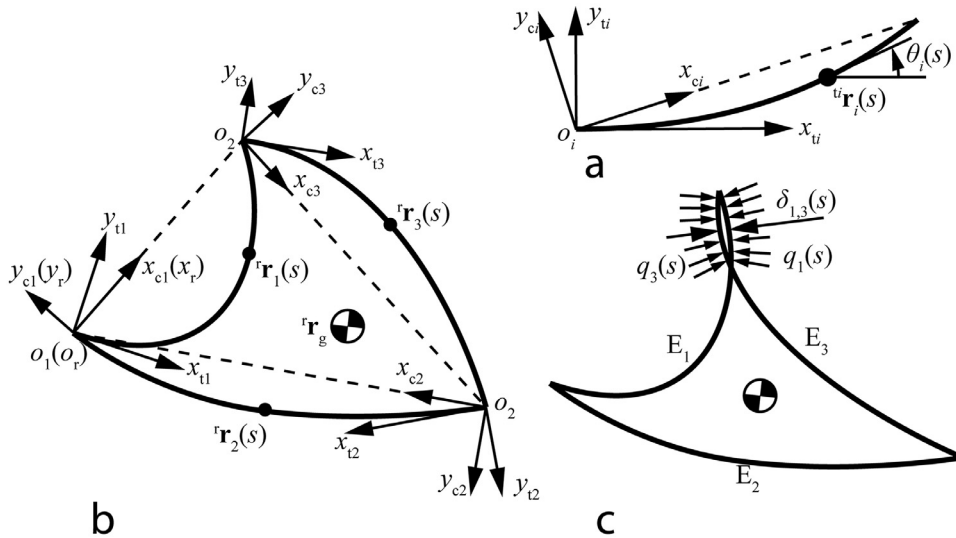


**Fig. 5.** Rolling kinematics of the triangular closed-chain soft robot.

layer (Fig. 1a).  $f()$  is the cubic function expressed by Eq. (1).  ${}^tr_i(s)$  is the coordinate of the point at  $s$  with the components in the  $x_{ti}$ - $o_i$ - $y_{ti}$  coordinate system.

In addition to  $x_{ti}$ - $o_i$ - $y_{ti}$ , another Cartesian coordinate system (i.e.  $x_{ci}$ - $o_i$ - $y_{ci}$ ) is built with the  $x_{ci}$  axis through two ends of the actuator, which is called the transitional reference frame. The homogeneous transformation matrices from  $x_{ci}$ - $o_i$ - $y_{ci}$  to  $x_{ti}$ - $o_i$ - $y_{ti}$  and from  $x_{ci}$ - $o_i$ - $y_{ci}$  to  $x_{cj}$ - $o_j$ - $y_{cj}$  are calculated according to Eqs. (5) and (6) respectively.

$${}^{ci}\mathbf{T}_{ti} = \begin{pmatrix} \cos^{ci}\theta_{ti} & \sin^{ci}\theta_{ti} & 0 \\ -\sin^{ci}\theta_{ti} & \cos^{ci}\theta_{ti} & 0 \\ 0 & 0 & 1 \end{pmatrix} \quad (5)$$

$${}^{ci}\mathbf{T}_{cj} = \begin{pmatrix} \cos^{ci}\theta_{cj} & -\sin^{ci}\theta_{cj} & -D_j \cos^{ci}\theta_{cj} \\ \sin^{ci}\theta_{cj} & \cos^{ci}\theta_{cj} & -D_j \sin^{ci}\theta_{cj} \\ 0 & 0 & 1 \end{pmatrix} \quad (6)$$

where

$$\cos^{ci}\theta_{ti} = {}^tx_i(L)/D_i$$

$$\sin^{ci}\theta_{ti} = {}^ty_i(L)/D_i$$

$$\cos^{ci}\theta_{cj} = -\left(D_i^2 + D_j^2 - D_k^2\right)/2D_iD_j$$

$$\sin^{ci}\theta_{cj} = \sqrt{1 - \cos^{2ci}\theta_{cj}}$$

$$D_i = \sqrt{{}^tx_i(L)^2 + {}^ty_i(L)^2}$$

where  $i = 1, 2, 3$  is each actuator's number.  $L$  is the length of each actuator.  $D_i$  is the distance between any two vertexes of the triangle.

The coordinate system  $x_{cl}$ - $o_1$ - $y_{cl}$  is taken as the robot's reference frame, denoted as  $x_r$ - $o_r$ - $y_r$ . Then, the transformation matrices between  $x_{ti}$ - $o_i$ - $y_{ti}$  and  $x_r$ - $o_r$ - $y_r$  can be expressed as Eqs. (7)–(9). With these matrices, the point coordinate of the soft actuator can be transformed from the actuator's reference frame into the robot's reference frame, as expressed by Eq. (10). Therefore, the edge curves of the soft robot are obtained, i.e.  ${}^r r_i(s)$ . Provided that each edge with one soft actuator distributes its mass uniformly along the length, the mass center and radius of gyration can be determined, as expressed by Eqs. (11) and (12).

$${}^r\mathbf{T}_{t1} = {}^{cl}\mathbf{T}_{t1} \quad (7)$$

$${}^r\mathbf{T}_{t2} = {}^{cl}\mathbf{T}_{c2} {}^{c2}\mathbf{T}_{t2} \quad (8)$$

$${}^r\mathbf{T}_{t3} = {}^{c3}\mathbf{T}_{c1}^{-1} {}^{c3}\mathbf{T}_{t3} \quad (9)$$

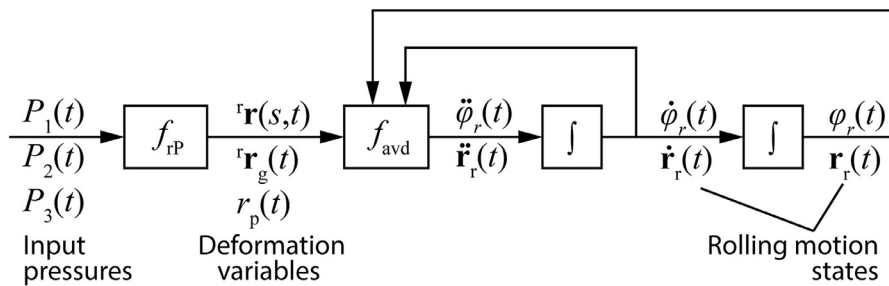


**Fig. 6.** Simulation scheme for deformation and rolling kinematics of the triangular closed-chain soft robot.  $f_{rp}$  is the function that calculates the profile, mass center and gyration radius of the robot according to the inflating pressure (Eq. (17)), and  $f_{avd}$  is the function that calculates linear and angular accelerations of the robot according to its velocities and displacements (Eq. (33)).

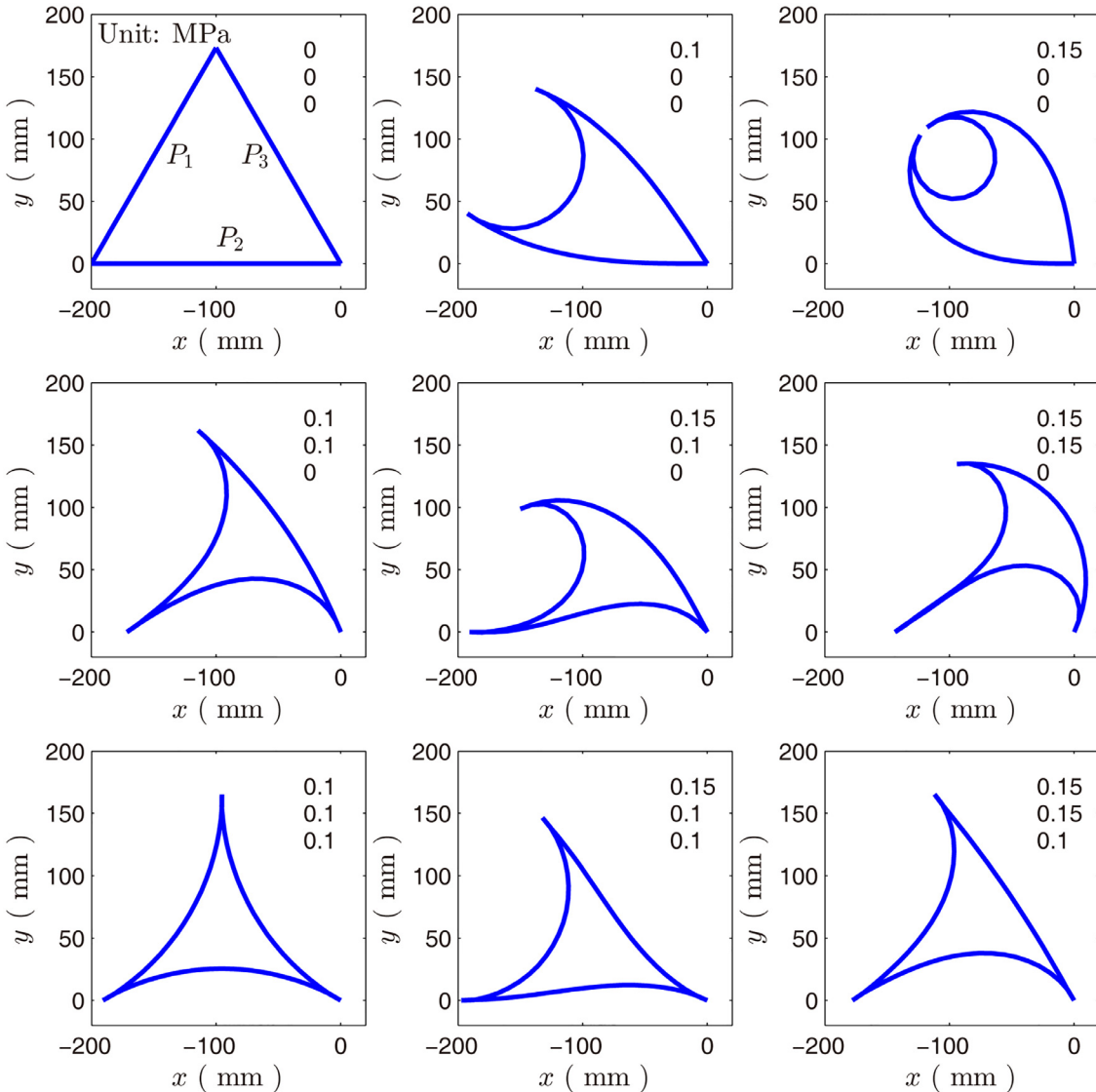


**Fig. 7.** Simulated deformation of the soft robot with different inflating pressures. The pressures are listed at the upper right of each image.

**Table 2**  
Mass center and gyration radius of the soft robot in simulation and experiment.

	Mass center $\bar{\mathbf{r}}_g$ (mm)			Gyration radius $r_p$ (mm)		
	Simulation	Experiment	Error	Simulation	Experiment	Error
1	(99.98, -57.74)	(93.93, -57.71)	5.49%	83.67	78.66	6.37%
2	(56.97, -67.66)	(55.24, -65.07)	3.65%	69.76	72.49	-3.77%
3	(74.14, -61.54)	(73.97, -70.61)	8.87%	59.18	58.30	1.51%
4	(88.04, -62.33)	(85.15, -67.40)	5.37%	68.93	70.52	-2.25%
5	(75.32, -71.28)	(69.94, -72.74)	5.52%	65.99	64.91	1.66%
6	(87.53, -61.08)	(81.63, -67.05)	7.95%	63.86	66.70	-4.26%
7	(85.40, -65.08)	(83.38, -65.43)	1.93%	70.96	70.25	1.01%
8	(80.21, -69.14)	(73.07, -73.34)	8.00%	70.18	63.82	9.97%
9	(80.58, -61.39)	(78.88, -67.93)	6.49%	70.37	65.65	7.19%

$$\bar{\mathbf{r}}_i(s) = {}^r\mathbf{T}_{ti}{}^U\bar{\mathbf{r}}_i(s) \quad (10)$$

$${}^r\mathbf{r}_g = \frac{1}{3L} \sum_{i=1}^3 \int_0^L {}^r\mathbf{r}_i(s) ds \quad (11)$$

$$r_p = \sqrt{\frac{1}{3L} \sum_{i=1}^3 \int_0^L \| {}^r\mathbf{r}_i(s) - {}^r\mathbf{r}_g \|^2 ds} \quad (12)$$

where the point coordinate with a bar above means its homogeneous form, i.e.  $\bar{\mathbf{r}} = [\mathbf{r}^T, 1]^T$ .

To sum up, according to Eqs. (3)–(10), the edge curves of the soft robot can be derived from the bending curvatures of the three edges, whose expression is denoted as  $f_{rk}$  in Eq. (13). However, according to Eq. (2),  $\kappa_i(s)$  has not been determined since the bending moment  $M_i(s)$  is unknown. Therefore, it is still necessary to derive  $M_i(s)$  from  ${}^r\mathbf{r}_i(s)$ , whose expression is denoted as  $f_{Mr}$  in Eq. (14), to make the equations

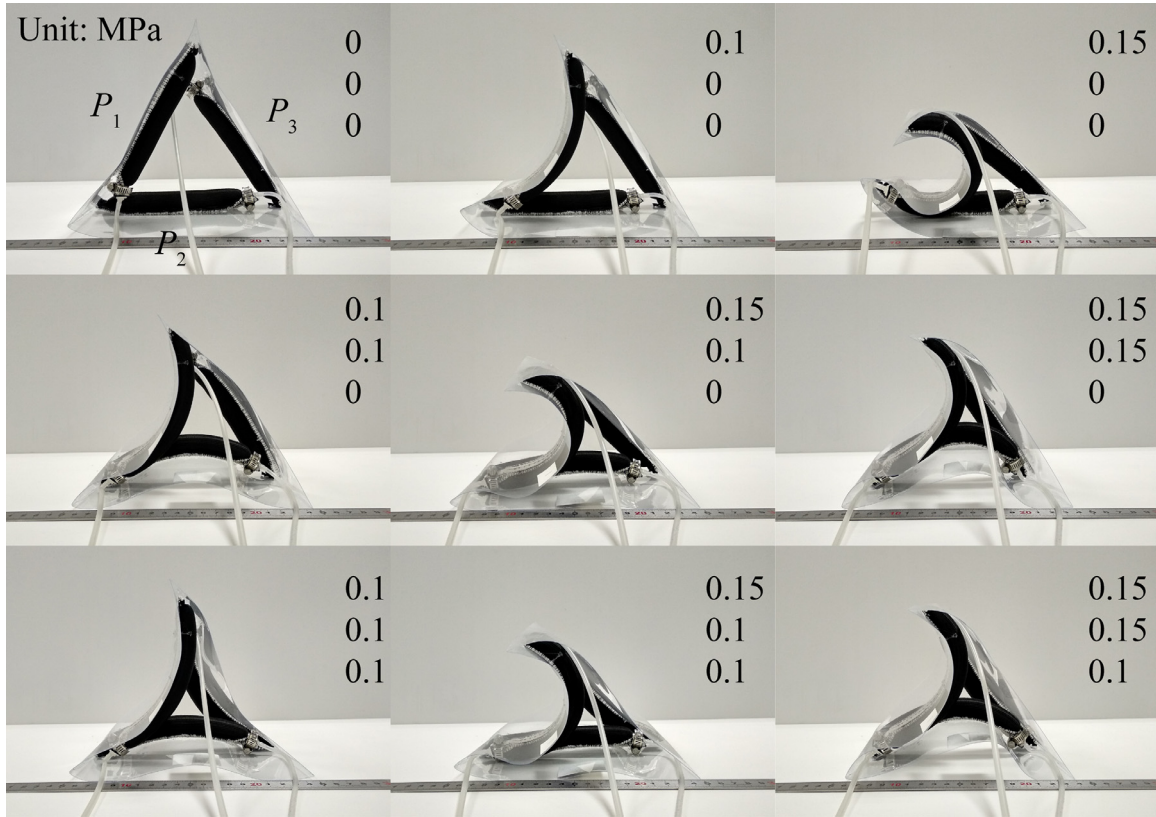


**Fig. 8.** Experimental deformation of the soft robot with different inflating pressures. The pressures are listed at the upper right of each image.

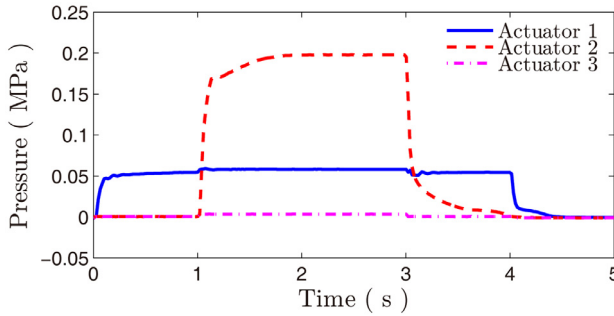


**Fig. 9.** Inflating pressure of the soft actuators during a rolling cycle. The actuators have been numbered in Fig. 8.

closed. As shown in Fig. 4c, if any two edges have interference with each other, each edge will be exerted by a distributed interactive contact force, denoted as  $q_i(s)$ . Since this contact force is normal to each edge, the bending moment can be obtained according to Eq. (15). Magnitude of the contact force depends on the interference depth  $\delta_i(s)$  and the contact stiffness  $k$ , as expressed by Eq. (16), in which  $\delta_i(s) \leq 0$  means no interference occurs. Since  $\delta_i(s)$  is determined by  $^r\mathbf{r}_i(s)$ ,  $M_i(s)$  can be derived from  $^r\mathbf{r}_i(s)$  according to Eqs. (15) and (16).

$$[^r\mathbf{r}_1(s), ^r\mathbf{r}_2(s), ^r\mathbf{r}_3(s)] = f_{rk} [\kappa_1(s), \kappa_2(s), \kappa_3(s)] \quad (13)$$

$$[M_1(s), M_2(s), M_3(s)] = f_{Mr} [^r\mathbf{r}_1(s), ^r\mathbf{r}_2(s), ^r\mathbf{r}_3(s)] \quad (14)$$

$$M_i(s) = \frac{s}{L} \int_0^L \int_0^s q_i(s) ds ds - \int_0^s \int_0^s q_i(s) ds ds \quad (15)$$

$$q_i(s) = \begin{cases} k\delta_i(s), & \delta_i(s) > 0 \\ 0, & \delta_i(s) \leq 0 \end{cases} \quad (16)$$

Solving combination of Eqs. (2), (13) and (14),  $\kappa_i(s)$  and  $^r\mathbf{r}_i(s)$  can be determined. Furthermore, the mass center and gyration radius can also be calculated according to Eqs. (11) and (12). By varying the actuators' inflating pressures  $P_i$  with time, the time-varying profile, mass center and gyration radius of the soft robot can be obtained, whose expression is denoted as  $f_{rp}$  in Eq. (17). Here, the profile is the concatenation of the three edge curves, as expressed by Eq. (18).

$$[^r\mathbf{r}(s, t), ^r\mathbf{r}_g(t), r_p(t)] = f_{rp} [P_1(t), P_2(t), P_3(t)] \quad (17)$$

$$^r\mathbf{r}(s, t) = \begin{cases} ^r\mathbf{r}_1(s), & 0 \leq s < L \\ ^r\mathbf{r}_3(s - L), & L \leq s < 2L \\ ^r\mathbf{r}_2(s - 2L), & 2L \leq s < 3L \end{cases} \quad (18)$$

where  $t$  is the time.

### 3.3. Rolling dynamics

In above analysis, the profile, mass center and gyration radius of the soft robot have been derived from the inflating pressures of the soft actuators, whose final result is expressed by Eq. (17). Based on that, the robot's rolling dynamics is further analyzed, as shown in Fig. 5. The coordinates of the profile and mass center can be transformed from the body reference frame  $x_r$ - $y_r$ - $z_r$  into the ground one  $x$ - $y$  according to Eqs. (19) and (20) respectively. The velocity of the profile can be obtained from Eq. (22), and the acceleration of the mass center can be calculated according to Eq. (23).

$$\mathbf{r}(s, t) = \mathbf{R}_r(t)^T \mathbf{r}(s, t) + \mathbf{r}_r(t) \quad (19)$$

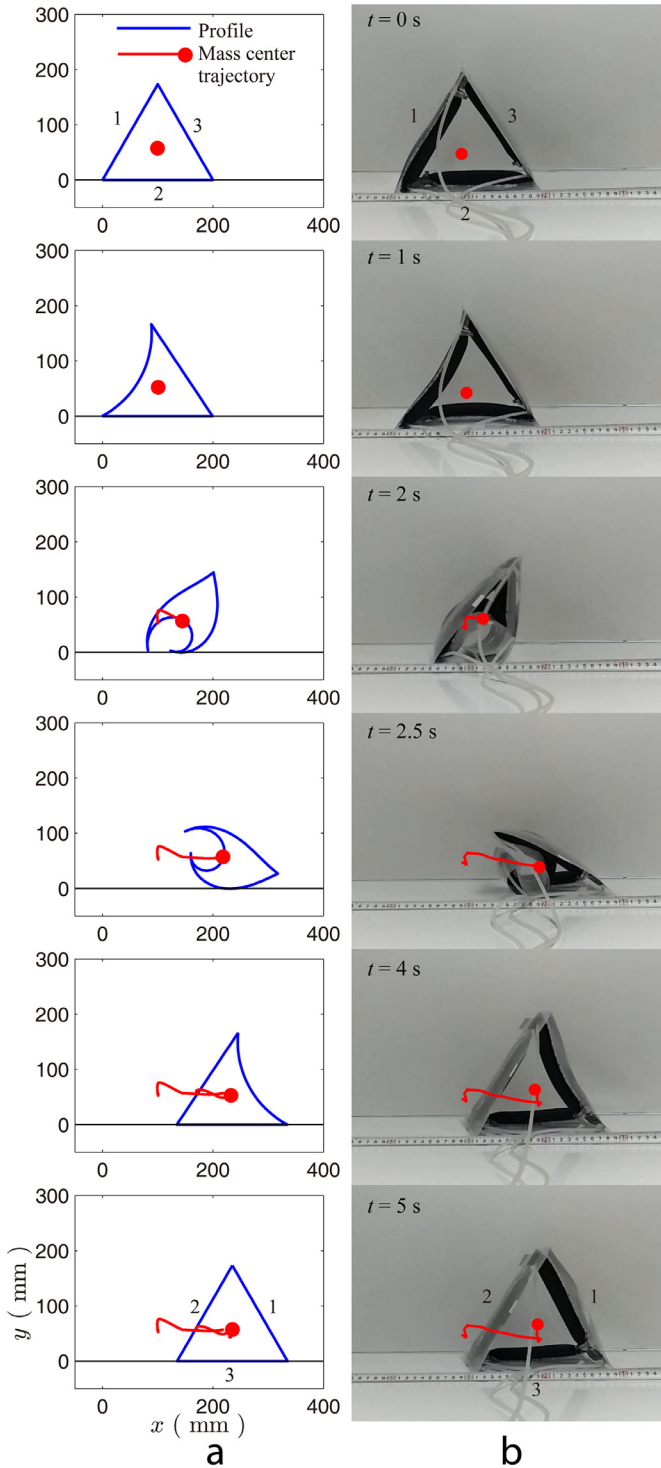


**Fig. 10.** Rolling locomotion cycle of the proposed soft robot in (a) simulation and (b) experiment on level ground.

$$\mathbf{r}_g(t) = \mathbf{R}_r(t)^T \mathbf{r}_g(t) + \mathbf{r}_r(t) \quad (20)$$

$$\mathbf{R}_r(t) = \begin{pmatrix} \cos \varphi_r(t) & -\sin \varphi_r(t) \\ \sin \varphi_r(t) & \cos \varphi_r(t) \end{pmatrix} \quad (21)$$

$$\dot{\mathbf{r}}(s, t) = \frac{\partial \mathbf{R}_r}{\partial \varphi} \dot{\varphi}_r(t)^T \mathbf{r}(s, t) + \mathbf{R}_r(t)^T \dot{\mathbf{r}}(s, t) + \dot{\mathbf{r}}_r(t) \quad (22)$$

$$\ddot{\mathbf{r}}_g(t) = \left[ -\mathbf{R}_r \dot{\varphi}_r(t)^2 + \frac{\partial \mathbf{R}_r}{\partial \varphi} \dot{\varphi}_r(t) \right] \mathbf{r}_g(t) + 2 \frac{\partial \mathbf{R}_r}{\partial \varphi} \dot{\varphi}_r(t)^T \dot{\mathbf{r}}_g(t) + \mathbf{R}_r(t)^T \ddot{\mathbf{r}}_g(t) + \ddot{\mathbf{r}}_r(t) \quad (23)$$

To calculate the contact force between the robot and ground, it is necessary to find out the contact points first. The points on the robot's profile and under the horizontal line (i.e.  $x$ -axis in Fig. 5) are taken as the contact points, whose arc length coordinates compose a set  $S_c$ , as expressed by Eq. (24). Then, the contact force  $\mathbf{F}_c(t)$  can be calculated according to Eqs. (25)–(28), and the equivalent contact point  $\mathbf{r}_c(t)$  can be obtained from Eq. (29).

$$S_c = \{s | r_y(s, t) < 0\} \quad (24)$$

$$\mathbf{F}_c(t) = [F_t(t), F_n(t)]^T \quad (25)$$

$$F_n(t) = \int_{S_c} f_n(s, t) ds, \quad F_t(t) = \int_{S_c} f_t(s, t) ds \quad (26)$$

$$f_n(s, t) = -k_n r_y(s, t) - c_n \dot{r}_y(s, t) \quad (27)$$

$$f_t(s, t) = -\mu f_n(t) \text{sgn}(\dot{r}_x(t)) - c_t \dot{r}_x(t) \quad (28)$$

$$\mathbf{r}_c(t) = \frac{1}{F_n} \int_{S_c} f_n(s, t) \mathbf{r}(s, t) ds \quad (29)$$

where  $F_t(t)$  and  $F_n(t)$  are the tangential and normal components of the contact force respectively while  $f_t(s, t)$  and  $f_n(s, t)$  are their distributions along the arc length  $s$ .  $r_x(s, t)$  and  $r_y(s, t)$  are the  $x$  and  $y$  components of  $\mathbf{r}(s, t)$  respectively.  $k_n$  and  $c_n$  are the normal contact stiffness and damping between the robot and ground respectively.  $\mu$  is the Coulomb frictional coefficient and  $c_t$  is the tangential contact damping. In this research,  $\mu$  and  $c_t$  are measured by the sliding experiment [28] with different sliding velocities,  $k_n$  is calculated according to the elastic modules of the PVC material by assuming a Hertzian contact condition [29], and  $c_n$  is adjusted in the simulation to ensure the computation convergence and stability.

According to the Newton–Euler theory, the linear and angular accelerations of the robot can be derived from the contact and gravity forces, as expressed by Eqs. (30) and (31). Substituting Eq. (30) into Eq. (23) yields Eq. (32), from which the acceleration of  $\varphi_r$  is obtained.

Eqs. (31) and (32) are the governing equations of the robot's rolling dynamics. On right side of Eq. (31),  $\mathbf{r}_c(t)$  is determined by  $\varphi_r(t)$ ,  $\mathbf{r}_r(t)$ ,  $\dot{\varphi}_r(t)$ ,  $\dot{\mathbf{r}}_r(t)$  and  $\ddot{\mathbf{r}}_r(t)$  according to Eqs. (19)–(22),(27),(29);  $\mathbf{r}_g(t)$  is determined by  $\varphi_r(t)$ ,  $\mathbf{r}_r(t)$  and  $\dot{\mathbf{r}}_g(t)$  according to Eqs. (20) and (21);  $\mathbf{F}_c(t)$  is determined by  $\varphi_r(t)$ ,  $\mathbf{r}_r(t)$ ,  $\dot{\varphi}_r(t)$ ,  $\dot{\mathbf{r}}_r(t)$  and  $\ddot{\mathbf{r}}_r(t)$  according to Eqs. (19), (21), (22) and (25)–(28). Therefore,  $\ddot{\varphi}_r(t)$  is determined by  $\varphi_r(t)$ ,  $\mathbf{r}_r(t)$ ,  $\dot{\varphi}_r(t)$ ,  $\dot{\mathbf{r}}_r(t)$ ,  $\ddot{\mathbf{r}}_r(t)$ ,  $\mathbf{r}(s, t)$ ,  $\dot{\mathbf{r}}_g(t)$  and  $r_p(t)$ . Similarly, in Eq. (32),  $\ddot{\mathbf{r}}_r(t)$  is also determined by these variables. This relationship is denoted as  $f_{\text{avd}}$  in Eq. (33), which is a multi-variable second order differential equation.

$$\ddot{\mathbf{r}}_g(t) = \mathbf{F}_c(t)/m + \mathbf{g} \quad (30)$$

$$\ddot{\varphi}_r(t) = \left[ [\mathbf{r}_c(t) - \mathbf{r}_g(t)] \times \mathbf{F}_c(t) \right]_z / \left[ m r_p^2(t) \right] \quad (31)$$

$$\ddot{\mathbf{r}}_r(t) = \frac{\mathbf{F}_c(t)}{m} + \mathbf{g} + \left[ \mathbf{R}_r \dot{\varphi}_r(t)^2 - \frac{\partial \mathbf{R}_r}{\partial \varphi} \dot{\varphi}_r(t) \right] \mathbf{r}_g(t) - 2 \frac{\partial \mathbf{R}_r}{\partial \varphi} \dot{\varphi}_r(t)^T \dot{\mathbf{r}}_g(t) - \mathbf{R}_r(t)^T \ddot{\mathbf{r}}_g(t) \quad (32)$$

$$[\ddot{\varphi}_r(t), \ddot{\mathbf{r}}_r(t)] = f_{\text{avd}} [\varphi_r(t), \mathbf{r}_r(t), \dot{\varphi}_r(t), \dot{\mathbf{r}}_r(t), \mathbf{r}(s, t), \dot{\mathbf{r}}_g(t), r_p(t)] \quad (33)$$

where  $m$  is total mass of the soft robot.  $\mathbf{g}$  is the gravitational acceleration, which is taken as  $[0, -9810 \text{ mm/s}^2]^T$  for rolling locomotion on level ground or others for inclined ground cases.

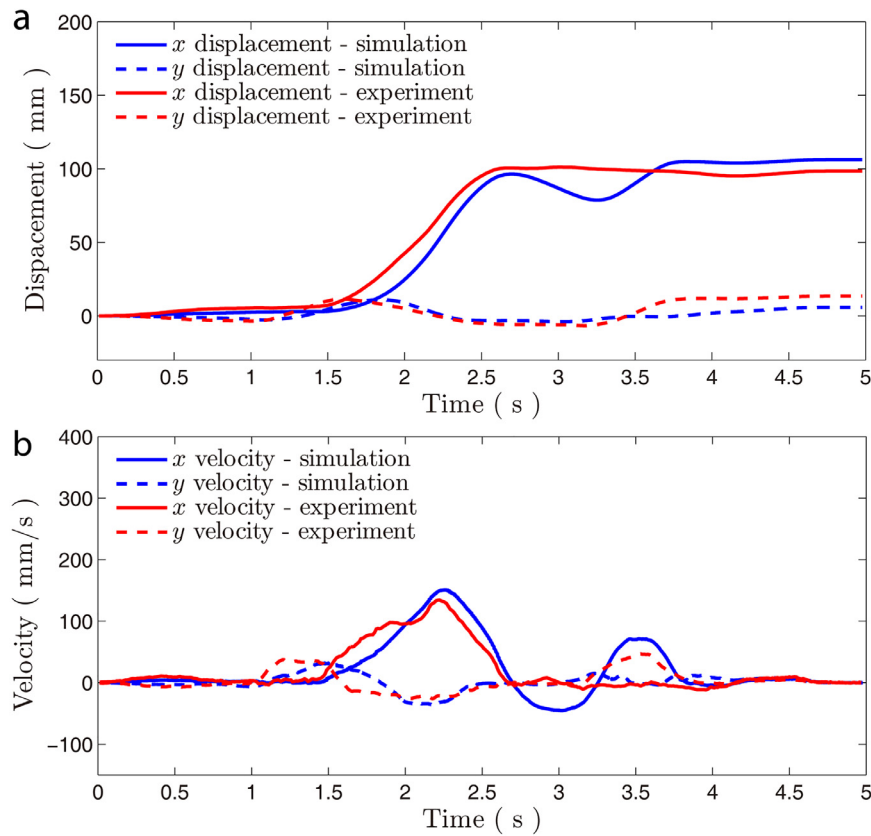


**Fig. 11.** Displacement and velocity of the robot's mass center during a rolling cycle on level ground.

### 3.4. Simulation scheme

By combining Eq. (17) with Eq. (33), a simulation scheme for the deformation and rolling dynamics of the soft robot is constructed, as shown in Fig. 6. According to it, a state-space model is built, as expressed by Eqs. (34)–(36). By MATLAB software, this model is coded as an S-function. During the simulation, the position and velocity of the mass center are calculated from the state variables according to Eqs. (20) and (22). Up to now, modeling of the locomotion kinematics and its simulation scheme have been completed. The simulation results will be discussed in the experiment section.

$$\text{States : } \mathbf{x}(t) = [\varphi_r(t), \mathbf{r}_r(t), \dot{\varphi}_r(t), \dot{\mathbf{r}}_r(t)] \quad (34)$$

$$\text{Inputs : } \mathbf{u}(t) = [P_1(t), P_2(t), P_3(t)] \quad (35)$$

$$\text{Equation : } \dot{\mathbf{x}}(t) = [\mathbf{x}_{3,4}(t), f_{\text{avd}}(\mathbf{x}(t), f_{\text{rp}}(\mathbf{u}(t)))] \quad (36)$$

where  $f_{\text{rp}}$  is the function that calculates the profile, mass center and gyration radius of the robot according to the inflating pressure, i.e. Eq. (17), and  $f_{\text{avd}}$  is the function that calculates the linear and angular accelerations of the robot according to its velocities, displacements and inflating pressures, i.e. Eq. (33).

## 4. Simulation and experimental results

This section presents the simulation and experiment on the deformation and rolling locomotion of the proposed soft robot. It is aimed to validate the robot's rolling capability and the model's effectiveness.

### 4.1. Deformation

In simulation, the deformation of the proposed soft robot is calculated by MATLAB according to Eq. (17). The robot's profiles in simu-

lation are shown in Fig. 7, which indicates that with different inflating pressures of the soft actuators, the robot deforms into different profiles. With single actuator inflated by 0.15 MPa, the robot can gather its two corners close. Comparing the simulated results with the experimental ones (Fig. 8), we find that the model can predict deformation of the soft robot effectively.

By extracting the profiles from Fig. 8, the experimental mass center and gyration radius in the robot's reference frame ( $x_r$ - $o_r$ - $y_r$  shown in Fig. 5) can be calculated according to Eqs. (11) and (12), and then they are compared with the simulated ones. In experiment, the robot is captured by a camera (Logitech<sup>®</sup>, Webcam C920) and then the captured image is binarized for tracing the boundary (i.e. the profile), based on which the mass center and gyration radius are calculated according to the pixels on the profile. To compensate the visual inference of the transparent membrane and pneumatic tubes with the soft actuators, the image is combined with the feature of uniform thickness of the soft actuators during the boundary tracing. The results of the mass center and gyration radius are listed in Table 2, which indicate that the maximum errors of the mass center and gyration radius are 8.87% and 9.97% respectively. The error is mainly caused by that the soft actuators obstruct the edges from contacting closely and distribute some mass of the robot offset the edges. By using some thinner soft actuators such as the electroactive polymer actuators [26] to construct the prototype, the error can be reduced.

### 4.2. Rolling locomotion

Rolling locomotion of the proposed soft robot is simulated in MATLAB Simulink by constructing the state-space model according to Eqs. (34)–(36) and Fig. 6. The simulation time of a rolling cycle is set as 5 s. Two cases are considered: 1) rolling on level ground and 2) rolling on inclined ground. Their only difference in simulation is the direction of the gravitational acceleration in Eq. (32).

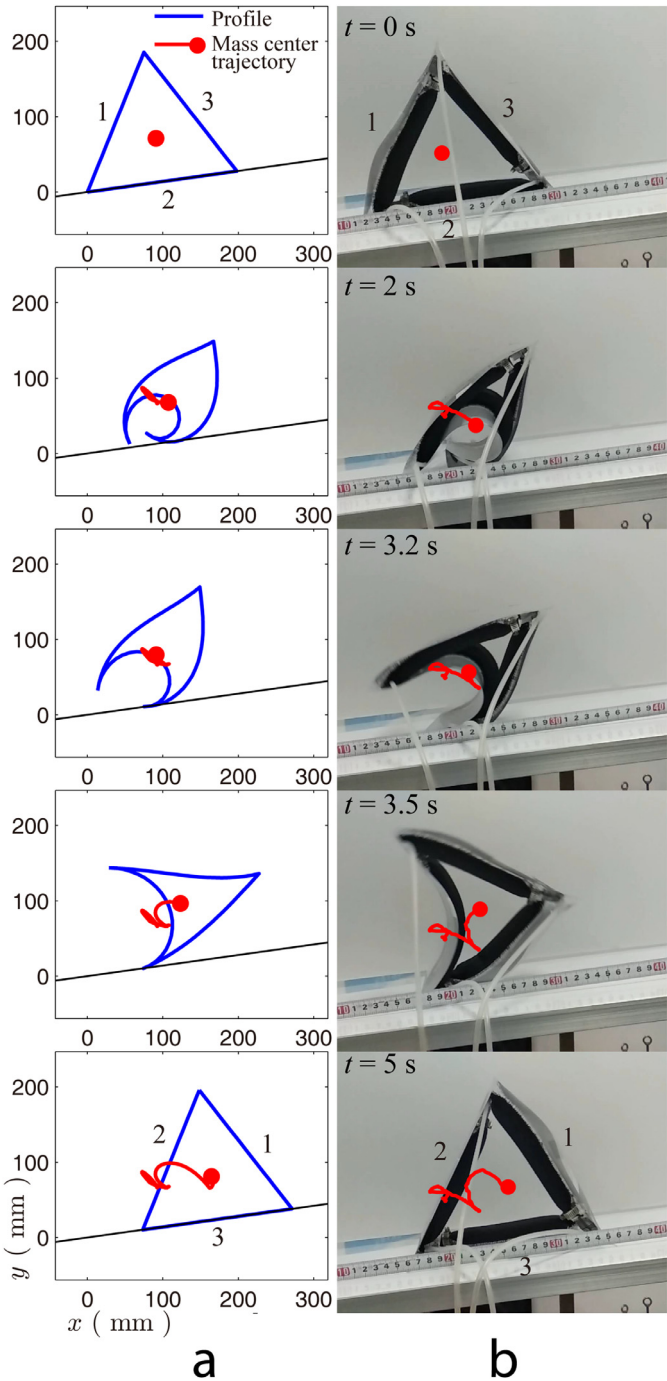


**Fig. 12.** Rolling locomotion cycle of the proposed soft robot in (a) simulation and (b) experiment on inclined ground with slope of 8°

To ensure that the simulation has the same input signals as the experiment, the model is fed with the inflating pressures that are obtained from the experiment by three pressure sensors (XGZP6847200KPG, 0–200 kPa, 0–5 V), as shown in Fig. 9. According to the pressure curves, the time scheme of the locomotion cycle is indicated, i.e. 0–1 s for the stiffening phase, 1–2 s for the gathering phase, 2–3 for the rolling phase and 3–5 for the releasing phase. During the releasing phase, Actuator 2 is released in 3–4 s while Actuator 1 is released in 4–5 s. The pressure for stiffening Actuator 1 is 0.06 MPa while that for bending Actuator 2 is 0.2 MPa.

During the simulation, the robot's profile is calculated from the input signal and state variables according to Eqs. (17) and (19), and the position and velocity of the robot's mass center are calculated according to Eqs. (20) and (22). In the experiment, the robot's profile is captured by a camera and the mass center is calculated by the aforementioned image processing.

#### 4.2.1. Locomotion on level ground

The profiles and the mass center trajectories of the soft robot during the level-ground locomotion are shown in Fig. 10 (see Video\_1.avi and Video\_2.mp4), which indicates that the simulation is basically consistent with the experiment. The error between the simulation and experiment is evaluated by the Fréchet distance [30] between their mass center trajectories. In mathematics, the Fréchet distance between two curves is the length of the shortest line segment sufficient for both ends to traverse the two curves [31]. For the mass center trajectories, their Fréchet distance is computed by the discrete method [30], which results in 6.9%. During the rolling locomotion, the mass center is elevated first, then declined and last elevated again to the initial level, which draws a N-shaped trajectory with size of about 106 × 27 mm (simulation) and 100 × 25 mm (experiment) in the movement plane.

The displacement and velocity components are plotted in Fig. 11a and b respectively. The displacement and velocity curves indicate that the rolling locomotion has several features: 1) the horizontal displacement mainly occurs in the rolling phase (2–3 s) and secondly in the gathering phase (1–2 s); 2) the maximum horizontal velocity is reached in the rolling phase; 3) the mass center mainly undulates during the gathering phase and the early releasing phase (3–4 s).

According to Fig. 11, the simulation can predict the experimental motion in general. However, in detail, the simulation shows a back and forth rolling motion during 2.7–3.8 s while the experiment does not. It is because that the calculated profile is more similar to arc shape than the experimental one and thus make the robot easier to roll in simulation than in experiment (see Fig. 10). The proposed soft robot can roll forward by 106 mm and 100 mm per cycle of 5 s in simulation and experiment respectively, which indicates a rolling stride error of 6.0%. Their average velocities are about 21 mm/s and 20 mm/s respectively. The error between the simulation and experiment comes from several aspects: 1) in the prototype, the soft actuators of certain thickness change the ideal contact between edges of the membrane and the ideal mass distribution of the robot; 2) in detecting the experimental mass center, the image processing method induces some error; 3) in simulation, some parameters such as the Coulomb frictional coefficient measured from experiment may induce some error.

#### 4.2.2. Locomotion on inclined ground

In the inclined-ground rolling simulation and experiment, the same inflating pressures as in the level-ground case is applied to the soft actuators. By gradually increasing the slope angle of the ground with increment of 1°, it is found that the maximum slopes for normal rolling locomotion of the robot in simulation and experiment are both 8°. The simulation and experiment in this condition are shown in Figs. 12 and 13 (see Video\_3.avi and Video\_4.mp4).

Fig. 12 shows that the simulation and experiment produce similar profiles and mass center trajectories. The error of the mass trajectories between the simulation and experiment is calculated by the normalized Fréchet distance [30], which results in 9.4%. These trajectories resemble an anti-oblique lowercase *n* with size of 75 × 35 mm (simulation) and 76 × 38 mm (experiment). Compared with the level-ground rolling cases, the inclined ground reduces the locomotion displacement of the soft robot and increases the undulation of its mass center. By investigating the phases of the rolling locomotion cycle, it is observed that the robot does not roll during the rolling phase (2–3 s), and instead it rolls in the early releasing phase (3–4 s). This rolling motion is mainly achieved by straightening of Actuator 2, which induces undulation of the mass center and impact of the soft robot upon the ground.

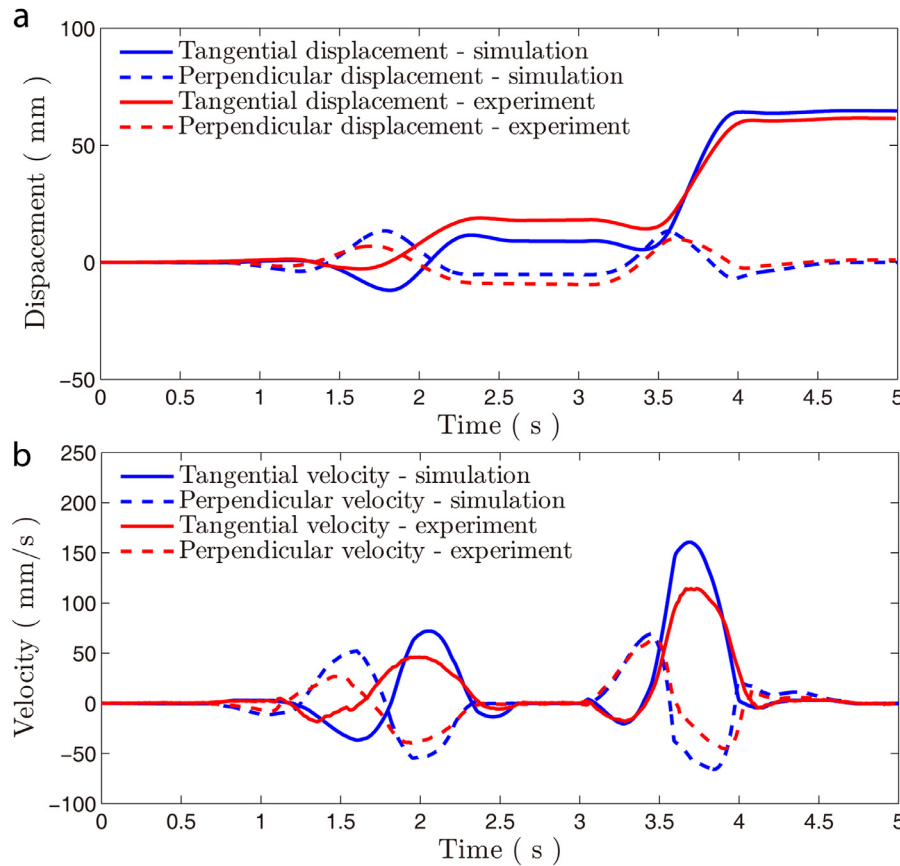


**Fig. 13.** Displacement and velocity of the robot's mass center during a rolling cycle on inclined ground of 8°. Tangential velocity means the velocity parallel with the inclined ground while the perpendicular velocity means velocity perpendicular to the ground.

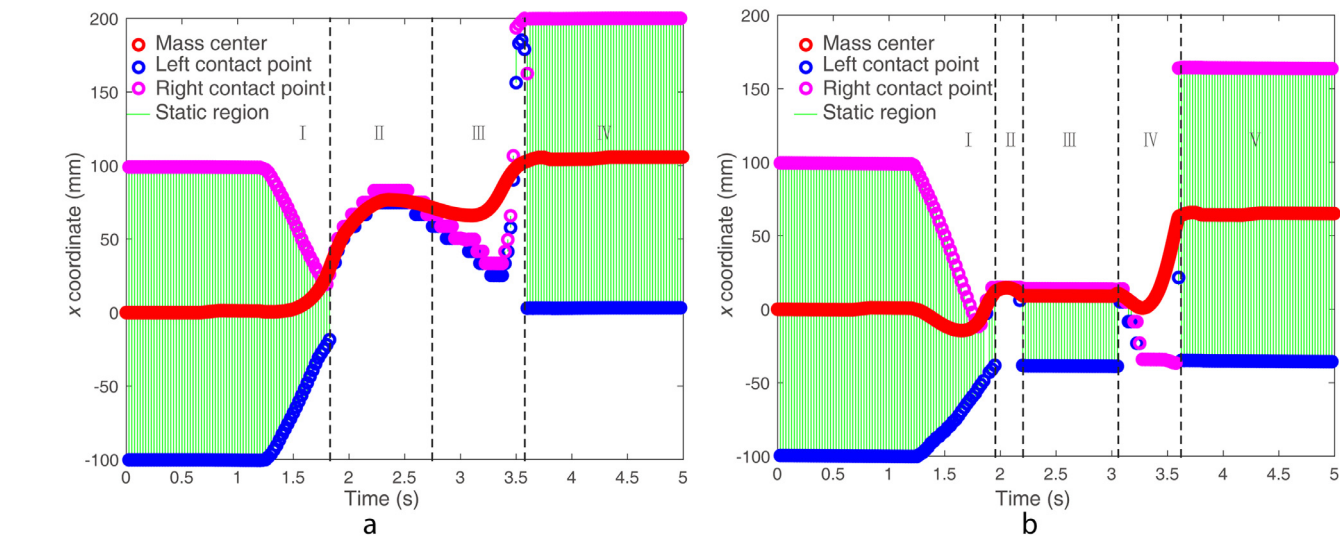


**Fig. 14.** Position of the robot's mass center and the contact points with the ground during one cycle of rolling locomotion (simulation result) (a) on level ground and (b) on slope.

From Fig. 13, several features of the rolling locomotion on inclined ground are observed: 1) the tangential (along the inclined plane) displacement mainly occurs in the early releasing phase (3–4 s) and secondly in the gathering phase (1–2 s); 2) the undulation of the mass center also mainly occurs in these phases; 3) the maximum tangential velocity is reached in the early releasing phase (3–4 s); 4) the tangential and perpendicular velocities basically have opposite signs, which indicates the n-shaped trajectories of the mass center in Fig. 12.

Fig. 13 also indicates the decent agreement between the simulation and experiment. In simulation and experiment, the rolling strides of the soft robot are 65 mm and 61 mm respectively, which indicate rolling velocities of 13 mm/s and 12 mm/s. The error between them is about 8%. Compared with the experiment, the simulation performs smaller displacement in the gathering phase (1–2 s) but larger in the early releasing phase (3–4 s). It is mainly caused by their slightly different profiles (see Fig. 12). About several cycles of rolling locomotion, please watch Video\_5.mp4 and Video\_6.mp4.

#### 4.2.3. Insight into the rolling locomotion

Observing position of the robot's mass center and the contact points with the ground (Fig. 14), we find that the state of the robot switches among three types during the rolling locomotion.

The first one is the static state, in which the robot locates its mass center between the left and right contact points and thus can perform the static movement that only depends on the robot's deformation and not influenced by its inertia. The regions labeled as I, IV in Fig. 14a and I, III, V in Fig. 14b are subjected to this state, which occupy the whole stiffening phase (Fig. 3a①-②), the early gathering phase (Fig. 3a②-③) and the later releasing phase (Fig. 3a⑤-⑥). Most of the crawling soft robots [11,32] are in the static state, whose movement can be stable and robust.

The second state is the transitional state, in which the robot is supported on the ground by single contact point (i.e. the left and right ones merged) whose position varies and approaches to the mass center when the robot rolls, shown as the regions II in Fig. 14a and b. Such state mainly occurs in the rolling phase (Fig. 3a③-④). Most of the wheel-like soft robots [9,20] are based on this transitional rolling motion, which can be smooth and efficient but the stability is vulnerable to the robot's inertia and the ground's slope.

The third state is the dynamic state, in which the robot uses its corner (a cusp point) to contact with the ground and behaves like an inverted pendulum, and the rolling movement is mainly determined by the robot's gravity and inertia. This state occurs in the regions III in Fig. 14a and IV in Fig. 14b or the early releasing phase (Fig. 3a④-⑤) in which the mass center deviates from the contact points. Some flipping robots [33] exploit such dynamic motions.

To sum up, during the rolling locomotion, the state of the proposed robot first transfers from static to transitional, then to dynamic and finally return to static again. In the three states, the robot performs movements as the crawling, wheel-like rolling and flipping robots respectively, i.e. combining good stability of the crawling and high efficiency of the rolling. However, from Figs. 10 and 12, it is observed that the robot's mass center performs significant vertical undulation during the rolling locomotion, that is 25 mm or 25% of the stride on level ground and 38 mm or 50% of the stride on slope of 8°, which causes larger energy expenditure (i.e. lower energy efficiency) than the current soft rolling robots [9,13,14] that have slighter rolling undulation. Nonetheless, lightweight features of the proposed robot can compensate part of the energy efficiency.

## 5. Potential and application

### 5.1. The tetrahedron morphology

As mentioned in Section 3.1, the proposed triangular soft robot is possible to be expanded into the parallel mechanism to enable the steering motion (Fig. 3b) or the tetrahedron mechanism to achieve the multi-direction movement (Fig. 3c). This section presents a preliminary model of the tetrahedron morphology and its simulation to verify the feasibility. The modeling process of the planar robot can be applied to the three-dimensional tetrahedron one with some modifications as follows.

First, all the aforementioned vectors and their operations are extended from 2D to 3D. Second, the soft actuators bend in their individual planes instead of coplanar with each other. As shown in Fig. 15a, the model assumes that each soft actuator bends in the plane (colored by transparent gray) defined by its two attached nodes and the middle point of the two non-attached nodes. This assumption is consistent with the symmetrical distribution of the soft actuators in the robot. Third, at each node, interference of the three intersected edges (i.e.  $i, j, k$  labeled in a right-hand order) is detected by the sign of the scalar triple product of their tangential vectors at this node, i.e.  $(\tau_i \times \tau_j) \cdot \tau_k$  in Fig. 15a, negative indicating interference, which is actually the 3D-form of that demonstrated in Fig. 4c. If the interference is detected, the interference depth of Edge  $i$  with respect to the plane defined by  $\tau_j$  and  $\tau_k$  is calcu-

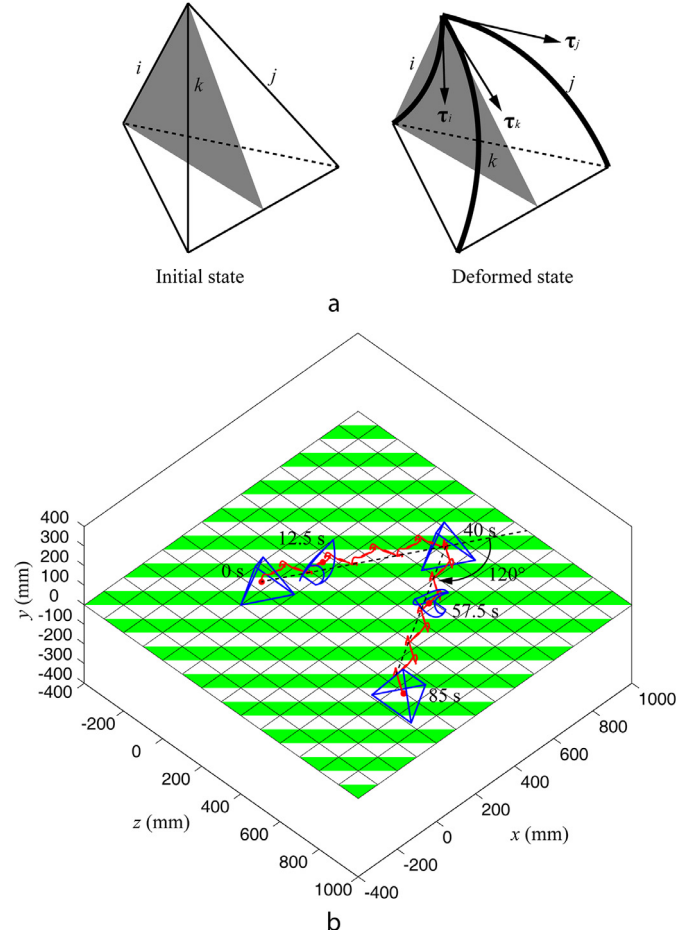


**Fig. 15.** A preliminary model of the soft rolling robot with a tetrahedron morphology. (a) The robot's deformation actuated by the soft bending actuators (b) The robot rolling in zig-zag path and turning right by 120° at middle of the path.

lated, based on which the interactive contact forces exerted on Edge  $i$  can be computed and aggregated to a boundary moment load according to Eqs. (15) and (16). The same case is with Edge  $j$  and  $k$ .

This tetrahedron model described above is implemented in the MATLAB software with the scheme shown in Fig. 6, and the input pressures take the same as those used in the planar model (Fig. 9) to drive the robot to roll with the cycle shown in Fig. 3c. Fig. 15 shows the simulation results, in which 17 locomotion cycles (or steps) are performed and the right turning of 120° is made at end of the 8th step. It can be observed that the robot can keep straight navigation but with a zig-zag path. It is because that the angle between the moving directions in two successive steps is only possibly 60°, -60° or 180° and cannot be the 0°, and thus the zig-zag path is actually achieved via alternately turning left and right by 60° (resulting in net turning angle of 0°). To change the moving direction, the robot should keep turning with different patterns from the zig-zag path in one or multiple successive steps, but the overall turning angle is always multiple of 60°. The right turning of 120° in Fig. 15b is actually achieved in two steps, each for 60°.

### 5.2. Navigation on rocky terrain

Due to the intrinsic flexibility, the proposed soft rolling robot is adaptable to unstructured environments such as ruins. Fig. 16 demonstrates rolling locomotion of the robot with the planar triangular morphology on a rocky terrain. The experimental result surprisingly indicates that the robot is able to move faster (with average velocity of 26 mm/s) on this rocky terrain than on plain ground, which is mainly

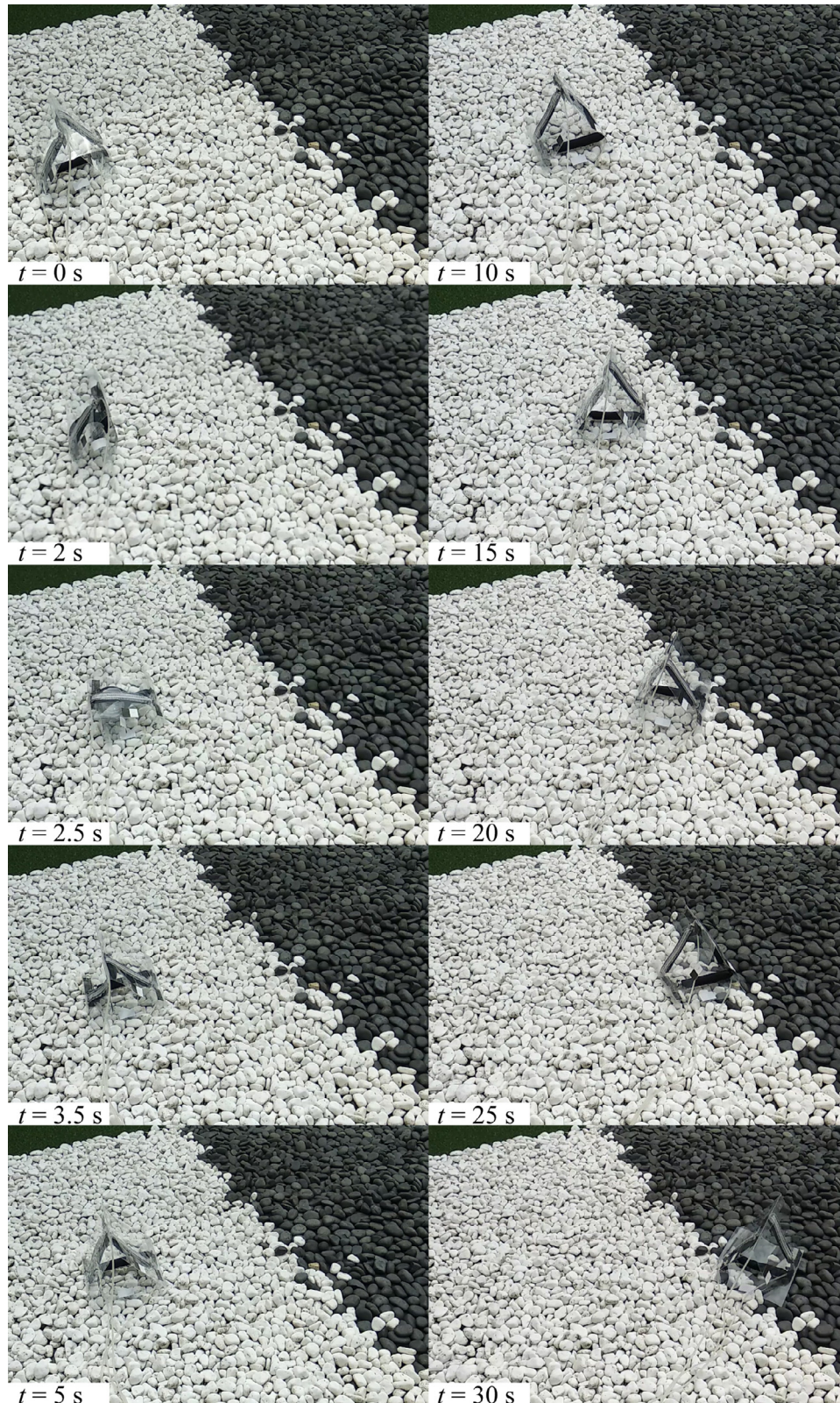


**Fig. 16.** Rolling locomotion of the proposed soft robot on the rocky terrain. Six cycles of rolling are shown. Average size of the rocks is 30 mm.

contributed by the crawling motion in the gathering phase (Fig. 3②–③). Despite higher speed, significant deviation of the moving direction is observed especially when the robot moves far, which is due to stumbling of the pneumatic pipes by the rocks. Therefore, it is essential to make the robot untethered, which will be considered in our future work.

## 6. Discussion and conclusions

This work mainly presents modeling, simulation and experiment of a novel triangular closed-chain soft rolling robot. The proposed robot uses only three soft actuators, which reduces its size and weight significantly.

The simulation and experimental results indicate that the state-space model, based on the continuous deformation and the rolling dynamics, can predict locomotion performances of the robot such as the mass center trajectories and average velocities effectively, within 10% of error. The proposed soft robot can perform the rolling locomotion with strides of 100–106 mm on level ground and 61–65 mm on 8° inclined ground, which indicates average velocities of 20–21 mm/s on level ground and 12–13 mm/s on 8° inclined ground.

However, there are still some aspects needed to be improved. First, the prototype is a little different from the proposed conceptual robot in the interference of edges and the distribution of mass, which induces the main error between the simulation and experiment. In future work, some thinner soft actuators such as the electroactive polymer actuators [26] will be considered to construct the prototype to reduce this error. Second, in experiment, some soft sensors and motion capturing methods will be introduced to replace the image processing method and thus improve the measurement accuracy of the mass center. Third, since the pneumatic pipe can have some influence on the rolling motion of the robot, we will consider to make it untethered by integrating a mini air source on it, of course at the cost of increasing the weight and reducing the speed. Two possible methods of including an air pump are considered: 1) use three soft springs with one end attached at the three corners of the robot to suspend the pump, 2) place three mini pumps at the three corners of the robot. The former only needs one pump but disturbs the original variation of the robot's mass center, which may add difficulty to the modeling. The latter can ensure certainty of the mass center and may enhance stability of the robot, but it needs more pumps and may change the tangential contact condition of the robot's side surfaces (i.e. interfere with the side surfaces). To overcome these challenges, future research may be needed especially on the fabrication and integration technologies.

Furthermore, we believe that the proposed soft robot has some other locomotion modes such as crawling, and it can also achieve turning motion by adding and differentially driving [32] another three soft actuators in parallel with the original ones. In addition, the 2D triangular closed-chain structure can be further expand to a 3D tetrahedron meshed structure for achieving 3D rolling locomotion. At the same time the model will be modified to simulate these cases. By scaling the proposed soft robot, it may be used in the space exploration and surgery.

## Supplementary material

Supplementary material associated with this article can be found, in the online version, at doi:[10.1016/j.mechatronics.2018.12.003](https://doi.org/10.1016/j.mechatronics.2018.12.003).

## References

- [1] Ilievski F, Mazzeo AD, Shepherd RF, Chen X, Whitesides GM. Soft robotics for chemists. *Angew Chem – Int Ed* 2011;50(8):1890–5.
- [2] Sanan S. Soft inflatable robots for safe physical human interaction, 3575511. Carnegie Mellon Univ.; 2013. p. 240.
- [3] Rodrigue H, Wang W, Han M-W, Kim TJY, Ahn S-H. An overview of shape memory alloy-coupled actuators and robots. *Soft Robot* 2017;4(1):3–15.
- [4] Shian S, Bertoldi K, Clarke D. Dielectric elastomer based ‘grippers’ for soft robotics. *Adv Mater* 2015;27.
- [5] Hughes J, Culha U, Giardina F, Guenther F, Rosendo A, Iida F. Soft manipulators and grippers: a review. *Front Robot AI* 2016;3:69.
- [6] Wehner M, et al. An integrated design and fabrication strategy for entirely soft, autonomous robots. *Nature* 2016;536(7617):451–5.
- [7] Mao S, et al. Gait study and pattern generation of a starfish-like soft robot with flexible rays actuated by SMAs. *J Bionic Eng* 2014;11(3):400–11.
- [8] Katschmann RK, DelPrete J, MacCurdy R, Rus D. Exploration of underwater life with an acoustically controlled soft robotic fish. *Sci Robot* 2018;3(16) eaar3449.
- [9] Onal CD, Rus D. A modular approach to soft robots. In: 2012 4th IEEE RAS EMBS international conference on biomedical robotics and biomechatronics (BioRob); 2012. p. 1038–45.

- [10] Nemirovski A, et al. Arthrobots. *Soft Robot* 2017 soro.2016.0043.
- [11] Wang W, Lee JY, Rodrigue H, Song SH, Chu WS, Ahn SH. Locomotion of inchworm-inspired robot made of smart soft composite (SSC). *Bioinspir Biomim* 2014;9(4).
- [12] Lin HT, Leish GG, Trimmer B, GoQBot: a caterpillar-inspired soft-bodied rolling robot. *Bioinspir Biomim* 2011;6(2).
- [13] Masuda Y, Ishikawa M. Development of a deformation-driven rolling robot with a soft outer shell. In: 2017 IEEE international conference on Advanced Intelligent Mechatronics (AIM); 2017. p. 1651–6.
- [14] Must I, Kaasik T, Baranova I, Johanson U, Punning A, Aabloo A. A power-autonomous soft-rolling wheel using ionic and capacitive actuators. *Int Soc Opt Photon* 2015;9430 Q:9430–9.
- [15] Matsumoto Y, Nakanishi H, Hirai S. Rolling locomotion of a deformable soft robot with built-in power source. In: Advances in mobile robotics – proceedings of the 11th international conference on climbing and walking robots and the support technologies for mobile machines, 2008. CLAWAR; 2008. p. 365–72.
- [16] Du Y, Xu M, Dong E, Zhang S, Yang J. A novel soft robot with three locomotion modes. In: 2011 IEEE international conference on robotics and biomimetics, ROBIO 2011; 2011. p. 98–103.
- [17] Correll N, Önal CD, Liang H, Schoenfeld E, Rus D. Soft autonomous materials—using active elasticity and embedded distributed computation. In: Springer tracts in advanced robotics, 79; 2014. p. 227–40.
- [18] Steltz E, Mozeika A, Rodenberg N, Brown E, Jaeger HM. JSEL: jamming skin enabled locomotion. In: in: 2009 IEEE/RSJ international conference on intelligent robots and systems, IROS 2009; 2009. p. 5672–7.
- [19] Koizumi Y, Shibata M, Hirai S. Rolling tensegrity driven by pneumatic soft actuators. In: Proceedings – IEEE international conference on robotics and automation; 2012. p. 1988–93.
- [20] Sugiyama Y, Shiotsu A, Yamanaka M, Hirai S. Circular/spherical robots for crawling and jumping. In: Proceedings – IEEE international conference on robotics and automation, 2005; 2005. p. 3595–600.
- [21] Matsuyama Y, Hirai S. Analysis of circular robot jumping by body deformation. In: Proceedings – IEEE international conference on robotics and automation; 2007. p. 1968–73.
- [22] Fei Y, Xu H. Modeling and motion control of a soft robot. *IEEE Trans Ind Electron* 2017;64(2):1737–42.
- [23] Noritsugu T, Yamamoto H, Sasakil D, Takaiwa M. Wearable power assist device for hand grasping using pneumatic artificial rubber muscle. In: SICE 2004 annu. conf., vol. 1; 2004. p. 420–5.
- [24] Andrikopoulos G, Nikolakopoulos G, Manesis S. A survey on applications of pneumatic artificial muscles. In: 2011 19th mediterranean conference on control and automation, MED 2011; 2011. p. 1439–46.
- [25] Al-Faham H, Davis S, Nefti-Meziani S. Wrist rehabilitation exoskeleton robot based on pneumatic soft actuators. In: 2016 international conference for students on applied engineering, ICSAE 2016; 2017. p. 491–6.
- [26] Bar-Cohen Y, Zhang Q. Electroactive polymer actuators and sensors. *MRS Bull* 2008;33(03):173–81.
- [27] Yim S, Sitti M. Design and rolling locomotion of a magnetically actuated soft capsule endoscope. *IEEE Trans Robot* 2012;28(1):183–94.
- [28] Gratton LM, Defrancesco S. A simple measurement of the sliding friction coefficient. *Phys Educ* 2006.
- [29] Thornton C, Ning Z, Wu C, Nasrullah M, Li L-Y. Contact mechanics and coefficients of restitution. *Granul Gases* 2001.
- [30] Eiter T, and Mannila H, “Computing discrete Fréchet distance,” 1994.
- [31] Wikipedia contributors. Fréchet distance — {Wikipedia} {,} The Free Encyclopedia [https://en.wikipedia.org/w/index.php?title=Fréchet\\_distance&oldid=822953337](https://en.wikipedia.org/w/index.php?title=Fréchet_distance&oldid=822953337).
- [32] Wu P, Jiangbei W, Yanqiong F. The structure, design, and closed-loop motion control of a differential drive soft robot. *Soft Robot* 2017 soro.2017.0042.
- [33] Geng T, Xu X, Yang Y, Li X, Zhang X. Designing ballistic flipping gait for a one-legged robot. In: Proc. 2001 IEEE/RSJ int. conf. intell. robot. syst. expand. soc. role robot. Next Millenn. (Cat. No.01CH37180), vol. 2; 2001. p. 716–21.

**Jiangbei Wang** received the B.S. degree in mechanical design, manufacture and automation from Chongqing University, Chongqing, China, in 2016. He is currently working toward the M.S. degree in the Research Institute of Robotics, School of Mechanical Engineering, Shanghai Jiao Tong University, Shanghai, China (e-mail: J.B.Wang@sjtu.edu.cn).

**Yanqiong Fei** received the B.S. degree in machinery technology from Xi'an Technological University, Xi'an, China, in 1994, the M.S. degree in mechanic engineering from Southeast University, Nanjing, China, in 1998, and the Ph.D. degree in mechatronics from Shanghai Jiao Tong University, Shanghai, China, in 2002. She is currently a professor in the Research Institute of Robotics, School of Mechanical Engineering, Shanghai Jiao Tong University, Shanghai, China. Her research interests include the self-reconfigurable modular robots, soft robotics and intelligent manufacturing. She was a visiting scholar of Massachusetts Institute of Technology, Cambridge, Massachusetts, U.S. in 2010.09–2011.09 (e-mail: fyq.sjtu@163.com).

**Zhaoyu Liu** received the B.S. degree in Process Equipment and Control Engineering from Dalian University of Technology, Dalian, China, in 2017. He is currently working toward the Ph.D. degree in the Research Institute of Robotics, School of Mechanical Engineering, Shanghai Jiao Tong University, Shanghai, China (e-mail: lzy0422@sjtu.edu.cn).